LETTER

Optical detection of radio waves through a nanomechanical transducer

T. Bagci[1], A. Simonsen[1], S. Schmid[2], L. G. Villanueva[2], E. Zeuthen[1], J. Appel[1], J. M. Taylor[3], A. Sørensen[1], K. Usami[1], A. Schliesser[1] & E. S. Polzik[1]

Low-loss transmission and sensitive recovery of weak radio-frequency and microwave signals is a ubiquitous challenge, crucial in radio astronomy, medical imaging, navigation, and classical and quantum communication. Efficient up-conversion of radio-frequency signals to an optical carrier would enable their transmission through optical fibres instead of through copper wires, drastically reducing losses, and would give access to the set of established quantum optical techniques that are routinely used in quantum-limited signal detection. Research in cavity optomechanics[1,2] has shown that nanomechanical oscillators can couple strongly to either microwave[3–5] or optical fields[6,7]. Here we demonstrate a room-temperature optoelectromechanical transducer with both these functionalities, following a recent proposal[8] using a high-quality nanomembrane. A voltage bias of less than 10 V is sufficient to induce strong coupling[4,6,7] between the voltage fluctuations in a radio-frequency resonance circuit and the membrane's displacement, which is simultaneously coupled to light reflected off its surface. The radio-frequency signals are detected as an optical phase shift with quantum-limited sensitivity. The corresponding half-wave voltage is in the microvolt range, orders of magnitude less than that of standard optical modulators. The noise of the transducer—beyond the measured 800 pV Hz$^{-1/2}$ Johnson noise of the resonant circuit—consists of the quantum noise of light and thermal fluctuations of the membrane, dominating the noise floor in potential applications in radio astronomy and nuclear magnetic imaging. Each of these contributions is inferred to be 60 pV Hz$^{-1/2}$ when balanced by choosing an electromechanical cooperativity of $\sim$150 with an optical power of 1 mW. The noise temperature of the membrane is 300 K divided by the cooperativity. For the highest observed cooperativity of 6,800, this leads to a projected noise temperature of 40 mK and a sensitivity limit of 5 pV Hz$^{-1/2}$. Our approach to all-optical, ultralow-noise detection of classical electronic signals sets the stage for coherent up-conversion of low-frequency quantum signals to the optical domain[8–11].
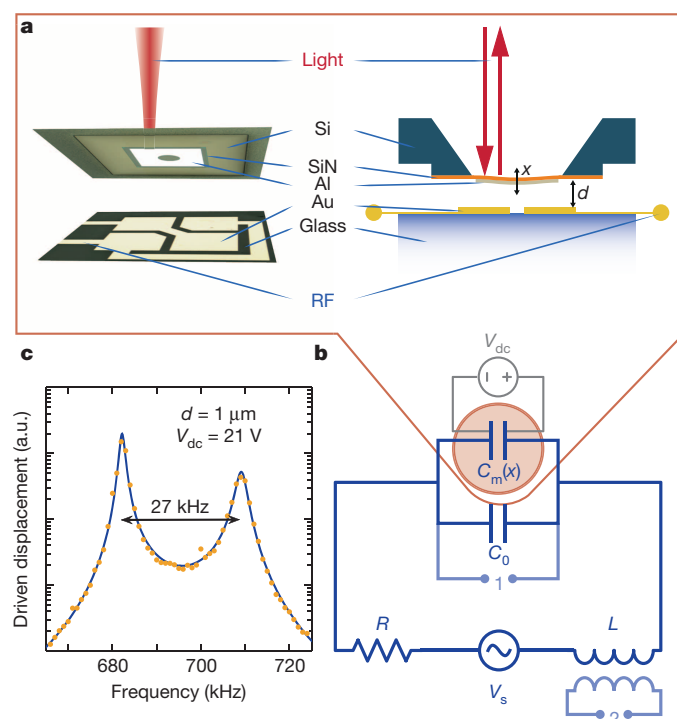
Optomechanical and electromechanical systems[1,2] have gained considerable attention recently for their potential as hybrid transducers between otherwise incompatible (quantum) systems, such as photonic, electronic and spin degrees of freedom[2,10,12]. The mechanical coupling of radio-frequency or microwave signals to optical fields is particularly attractive for present-day and future quantum technologies. Photon–phonon transfer protocols viable all the way to the quantum regime have already been implemented separately in the radio- and optical-frequency domains[7,13,14].

Among the optomechanical systems that have been considered for radio-to-optical transduction[8–10,15], we choose an approach[8] based on a nanomembrane[16,17] with a high quality factor, $Q_m \approx 3 \times 10^5$, which is coupled capacitively[18] to a radio-frequency resonance circuit (Fig. 1). Together with a four-segment gold electrode, the membrane forms a capacitor, whose capacitance, $C_m(x)$, depends on the membrane–electrode distance, $d + x$. With a tuning capacitor C_0, the total capacitance, $C(x) = C_0 + C_m(x)$, forms a resonance circuit with a typical

quality factor $Q_{LC} = \sqrt{L/C}/R = 130$ using a custom-made coil wired on a low-loss ferrite rod. This yields an inductance $L = 0.64$ mH and a loss $R \approx 20\,\Omega$. The circuit's resonance frequency $\Omega_{LC} = 1/\sqrt{LC}$ is tuned to the frequency, $\Omega_m/2\pi = 0.72$ MHz, of the fundamental drum mode of the membrane. The membrane–circuit system is coupled to a propagating optical mode reflected from the membrane.

The electromechanical dynamics is described most generically by the Hamiltonian[8]

$$H = \frac{\phi^2}{2L} + \frac{p^2}{2m} + \frac{m\Omega_m^2 x^2}{2} + \frac{q^2}{2C(x)} - qV_{dc} \qquad (1)$$

Figure 1 | Optoelectromechanical system. a, A 500-μm-square membrane of Al-coated[30] SiN in vacuum ($<10^{-5}$ mbar) forms a position-dependent capacitor, $C_m(x = 0) \approx 0.5$ pF, with a planar, four-segment gold electrode in the immediate vicinity ($0.9\,\mu m \lesssim d \lesssim 6\,\mu m$). The membrane electrode's potential is electrically floating. The membrane's displacement is converted into a phase shift of the laser beam reflected from the membrane. **b,** The membrane capacitor is part of an LC circuit, tuned to the mechanical resonance frequency by means of a tuning capacitor $C_0 \approx 80$ pF (Supplementary Information). A bias voltage, V_{dc}, couples the excitations of the LC circuit to the membrane's motion. The circuit is driven by a voltage V_s, which can be injected through the coupling port 2 or picked up by the inductor from the ambient radio-frequency (RF) radiation. **c,** For $d = 1\,\mu m$, the optically observed response of the membrane to a weak excitation of the system shows a split peak due to strong electromechanical coupling. a.u., arbitrary units.

[1]Niels Bohr Institute, University of Copenhagen, 2100 Copenhagen, Denmark. [2]Department of Micro- and Nanotechnology, Technical University of Denmark, DTU Nanotech, 2800 Kongens Lyngby, Denmark. [3]Joint Quantum Institute/NIST, College Park, Maryland 20742, USA.

where ϕ and q, respectively the flux in the inductor and the charge on the capacitors, are conjugate variables for the LC circuit, and x and p respectively denote the position and momentum of the membrane with an effective mass m. The last two terms represent the charging energy, $U_C(x)$, of the capacitors, which can be offset using an externally applied bias voltage, V_{dc} (Fig. 1). This energy, corresponding to the charge $\bar{q} = V_{dc}C(\bar{x})$, leads to a new equilibrium position, $\bar{x}$, for the membrane. Furthermore, the position-dependent capacitive force $F_C(x) = -dU_C/dx$ causes spring softening, reducing the membrane's motional eigenfrequency by $\Delta\Omega_m \approx -C''(\bar{x})V_{dc}^2/2m\Omega_m$ (ref. 19).

Much richer dynamics than this shift may be expected from the mutually coupled system described by equation (1). For small excursions, $(\delta q, \delta x)$, around the equilibrium, $(\bar{q}, \bar{x})$, it can be described by the linearized interaction term[8] (Supplementary Information)

$$H_I = G\delta q\delta x = \hbar g_{em}\frac{\delta q}{\sqrt{\hbar/2L\Omega_{LC}}}\frac{\delta x}{\sqrt{\hbar/2m\Omega_m}} \quad (2)$$

parameterized by either the coupling parameter $G = -V_{dc}C'(\bar{x})/C(\bar{x})$ or the electromechanical coupling energy, $\hbar g_{em}$, where $\hbar$ is Planck's constant (h) divided by 2π. This coupling leads to an exchange of energy between the electronic and mechanical subsystems at the rate g_{em}; if this rate exceeds their dissipation rates, respectively $\Gamma_{LC} = \Omega_{LC}/Q_{LC}$ and $\Gamma_m = \Omega_m/Q_m$, they hybridize into a strongly coupled electromechanical system[4,6,7]. Our system is deeply in the strong coupling regime ($2g_{em} = 2\pi \times 27$ kHz $> \Gamma_{LC} = 2\pi \times 5.5$ kHz $\gg \Gamma_m = 2\pi \times 20$ Hz) for a distance $d = 1$ μm and a bias voltage $V_{dc} = 21$ V (Fig. 1c). Here we detect the strong coupling using an independent optical probe on the mechanical system.

We have performed a series of experiments in which the bias voltage is systematically increased with a different sample, a larger distance, $d = 5.5$ μm, and a lower mechanical dissipation, $\Gamma_m/2\pi = 2.3$ Hz. The system is excited inductively through port 2 (Fig. 1b), inducing a weak radio-frequency signal of root mean squared amplitude $V_s = 670$ nV, at a frequency $\Omega \approx \Omega_{LC}$. The response of the coupled system can be measured both electrically, as the voltage across the capacitors (port 1 in Fig. 1b), and optically, by analysing the phase shift of a light beam (wavelength $\lambda = 633$ nm) reflected from the membrane. Both signals are recorded with a lock-in amplifier, which also provides the excitation signal.

The electrically measured response (Fig. 2a) shows the signature of a mechanically induced transparency[20], indicated by the dip in the LC resonance curve. Independently, we observe the radio-frequency signal in the LC circuit optically via the membrane mechanical dynamics (Fig. 2b). In particular, the electromechanical coupling leads to a broadening of the mechanical resonance to a new effective linewidth, $\Gamma_{eff} = (1 + \mathcal{C}_{em})\Gamma_m$, where $\mathcal{C}_{em}$ is the electromechanical cooperativity:

$$\mathcal{C}_{em} = \frac{4g_{em}^2}{\Gamma_m\Gamma_{LC}} \quad (3)$$

The width of the induced transparency dip and the mechanical linewidth grow in unison, and in agreement with our expectations, as $\Gamma_{eff} \propto V_{dc}^2$ (Fig. 2b, inset). Both of these features also shift to lower frequencies as the bias voltage is increased, following the expected $\Delta\Omega_m \propto -V_{dc}^2$ dependence[19]. We note that in each experiment we have tuned the LC resonance frequency to Ω_m.

Using the model based on the full Langevin equations (Supplementary Information), derived from the Hamiltonian in equation (1), we fit the electrically and optically measured curves, and for the two curves obtain fit parameters Ω_m, Ω_{LC}, Γ_{LC} and G that agree typically to within 1%. Together with the intrinsic damping determined independently from thermally driven spectra, the system's dynamics can be quantitatively predicted. Our data analysis allows us to quantify the coupling strength in three independent ways: analysis of the mechanical responses' spectral shape; comparison of the voltage and displacement modulation amplitudes; and in terms of the frequency
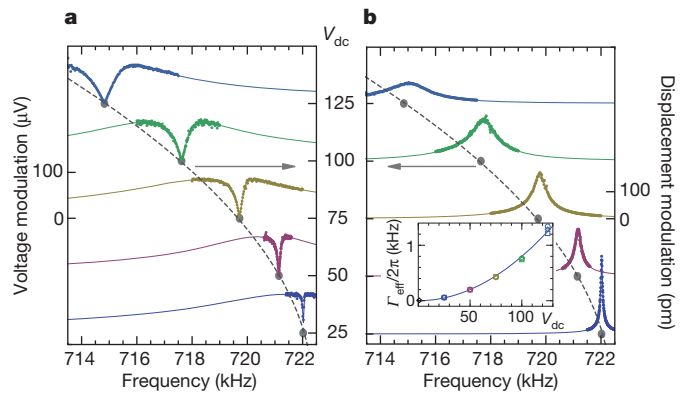
Figure 2 | Mechanically induced transparency. Response of the coupled system to a weak excitation at frequency Ω (through port 2 in Fig. 1b) probed through the voltage modulation in the LC circuit (at port 1) (**a**) and through the optical phase shift (**b**). The data (coloured dots) measured for five different bias voltages agree excellently with model fits (curves) respectively corresponding to $g_{em}/2\pi = 280, 470, 810, 1,030$ and $1,290$ Hz (from bottom to top). Each curve is offset so that its baseline corresponds to the V_{dc} indicated between the panels. Grey points indicate Ω_m values extracted for each set of data. A shift of $\Delta\Omega_m \propto -V_{dc}^2$ is fitted with the dashed line. Inset, effective linewidth of the mechanical resonance extracted from full model fits to the electrically (circles) and optically (boxes) measured response and simple Lorentzian fits to the optical data (diamonds). The solid line shows the expected $\Gamma_{eff} \propto V_{dc}^2$ scaling.

shift[19] of the mechanical mode. Finally, we compare these experimental values with a theoretical estimate accounting for the geometry of the electromechanical transducer. For $V_{dc} = 125$ V, we find that $G = 10.3$ kV m^{-1} following the first method, and similar values using the three others (Supplementary Information), demonstrating our thorough understanding of the system.

In another experimental run ($d = 4.5$ μm; Fig. 3), we characterized the strong electromechanical coupling[3,4,14] using the normal-mode splitting that gives rise to an avoided crossing of the resonances of the electronic circuit and the mechanical mode, as the latter is tuned through the former using the capacitive spring effect[19]. In contrast to earlier observations[4,6,7], we simultaneously witness the strong coupling through the optical readout, in which the recorded light phase reproduces the membrane motion (Fig. 3c, e). Again, the predictions derived from the Langevin equations are in excellent agreement with our observations, yielding a cooperativity of $\mathcal{C}_{em} = 3,800$ for these data with $m = 24$ ng and $\Gamma_m/2\pi = 3.1$ Hz.

We now turn to the performance of this interface as a radio-frequency/optical transducer. A relevant figure of merit for the purpose of bringing small signals onto an optical carrier is the voltage, V_π, required at the input of the series circuit to induce an optical phase shift of π. Achieving minimal V_π requires a balance between strong coupling and induced mechanical damping. For the optimal cooperativity, $\mathcal{C}_{em} = 1$, we find that

$$V_\pi = \frac{1}{2}\sqrt{mL\Gamma_m\Gamma_{LC}}\lambda\Omega_r \approx 140 \text{ μV} \quad (4)$$

at resonance ($\Omega_r \equiv \Omega_m = \Omega_{LC} = \Omega$), which is orders of magnitude below the corresponding figure of merit for not only commercial modulators optimized for decades by the telecom industry, but also explorative microwave photonic devices[21,22] based on electronic non-linearities. It is interesting to relate this performance to more fundamental entities, namely the electromagnetic field quanta that constitute the signal. Indeed it is possible to show that the quantum conversion efficiency, defined here as the ratio of optical sideband photons to the radio-frequency quanta extracted from the source, $V_s I/\hbar\Omega_{LC}$, for $\mathcal{C}_{em} \gg 1$, is given by (Supplementary Information)

$$\eta_{eo} = 4(kx_{zpf})^2\frac{\Phi_{car}}{\Gamma_m} \quad (5)$$
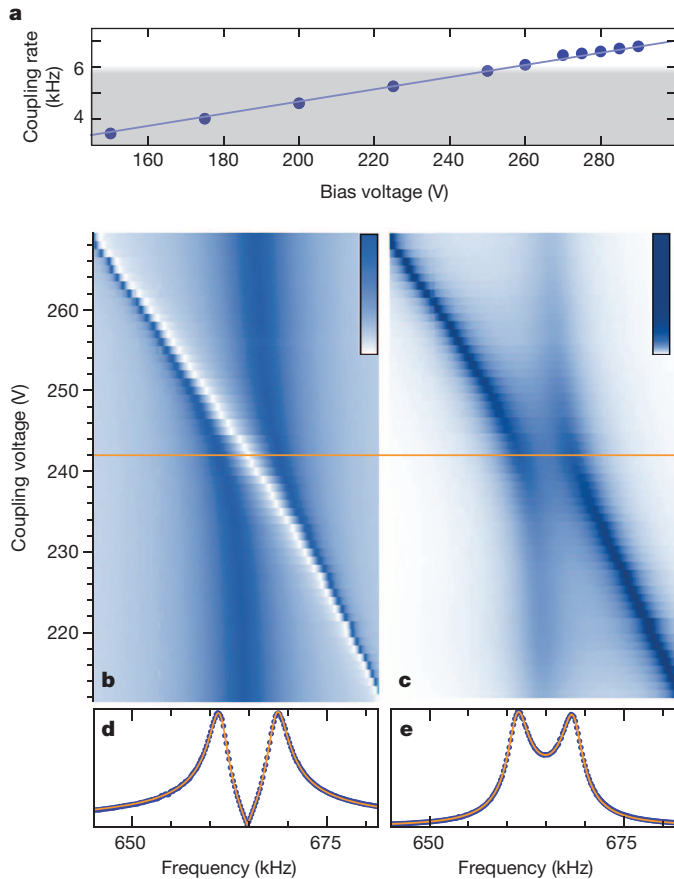
Figure 3 | Strong-coupling regime. a, Measured coherent coupling rate, $2g_{em}/2\pi$, as a function of bias voltage (points), and linear fit (line). The shaded area indicates the dissipation rate, $\Gamma_{LC}/2\pi \approx 5.9$ kHz of the LC circuit. **b–e**, Normalized response of the coupled system as measured on port 1 (Fig. 1c) (**b, d**) and via the optical phase shift induced by membrane displacements (**c, e**). The colour scales encode normalized voltage (**b**) and displacement modulation (**c**). On tuning of the bias voltage, the mechanical resonance frequency is tuned through the LC resonance, but owing to the strong coupling an avoided crossing is very clearly observed. Panels **d** and **e** show the spectra corresponding to the orange lines in **b** and **c**, at $V_{dc} = 242$ V, where the electronic and mechanical resonance frequencies coincide. Points are data; orange line is the model fit.

This corresponds to the squared effective Lamb–Dicke parameter, $(kx_{zpf})^2 = (2\pi/\lambda)^2 \hbar/2m\Omega_m$, enhanced by the number of photons sampling the membrane during the membrane excitations' lifetime (Φ_{car} is the photon flux and k is the wavenumber). For the experiments shown in Fig. 2, we deduce a conversion efficiency of 0.8% from the independently measured radio-frequency voltage and optical phase modulation. Although this result is limited by the optical power in this interferometer, we performed tests to confirm that the membranes can support optical readout powers of more than $\Phi_{car}hc/\lambda = 20$ mW without degradation of their (intrinsic) linewidth. We thus project that conversion efficiencies of the order of 50% are available. Note that this transducer constitutes a phase-insensitive amplifier, and can thus reach conversion efficiencies greater than one—at the expense of added quantum noise.

For the recovery of weak signals, the sensitivity and bandwidth of the interface is of greatest interest. The signal at the optical output of the device is the interferometrically measured spectral density of the optical phase, φ, of the light reflected from the membrane:

$$S_{\varphi\varphi}^{tot} = (2k)^2 |\chi_m^{eff}|^2 (|G\chi_{LC}|^2 S_{VV} + S_{FF}^{th}) + S_{\varphi\varphi}^{im} \quad (6)$$

The voltage V_s at the input of the resonance circuit (denoted here as its spectral density S_{VV}) is transduced to a phase shift via the circuit's susceptibility, χ_{LC}, the coupling, G, the effective membrane susceptibility,

χ_m^{eff}, and the optical wavenumber, k (Supplementary Information). The sensitivity is determined by the noise added within the interface. This includes, in particular, the imprecision in the phase measurement ($S_{\varphi\varphi}^{im}$) and the random thermal motion of the membrane induced by the Langevin force (S_{FF}^{th}). The former depends on the performance of the interferometric detector used and can be quantum limited ($S_{\varphi\varphi}^{im} \propto \Phi_{car}^{-1}$).

We demonstrate the sensitivity and the noise performance of the transduction scheme by measuring the noise as a function of the input circuit resistor and its temperature (Fig. 4). Because the home-made, high-Q inductor is too sensitive to the ambient radio-frequency radiation (Supplementary Information), we use a shielded commercial inductor (Picoelectronics) resulting in a lower value, $Q_{LC} = 47$, for these measurements. Red traces in Fig. 4a and Fig. 4b respectively present the optically measured noise spectrum and the corresponding voltage noise. On resonance, the dominant contribution is the Johnson
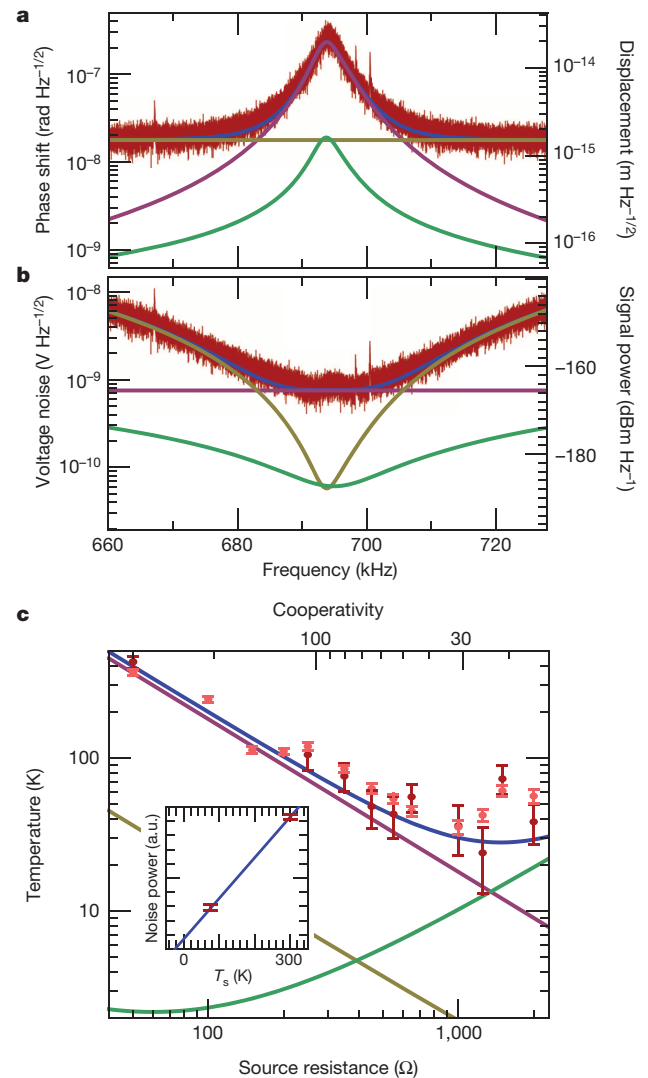
Figure 4 | Voltage sensitivity and noise. Noise characterization of the transducer with contributions from Johnson noise (violet), optical quantum phase noise (yellow) and membrane thermal noise (green). **a**, Optically measured noise (red) is well reproduced by a model $\sqrt{S_{\varphi\varphi}^{tot}}$ (blue). **b**, Data and models as in **a**, but divided by the interface's response function, $|\chi^{tot}|$, and thus referenced to the voltage, V_s, induced in the circuit. **c**, Noise temperature of the amplifier (errors, s.d.). It is determined using the Y-factor method, at the resonance frequency (dark red points), and in a 10-kHz-wide band around the resonance (light red points), as a function of external loading. Lines are the model of equation (7), broken down into contributions as in **a** and **b**. Inset, example of a noise temperature measurement at $R_s = 1,250$ Ω.

noise ($S_{VV}^{J} \approx (800 \text{ pV})^2 \text{ Hz}^{-1}$) of the circuit (violet). Off resonance, optical quantum (shot) noise (yellow) limits the phase sensitivity to $S_{\varphi\varphi}^{im} = (18 \text{ nrad})^2 \text{ Hz}^{-1}$, corresponding to membrane displacements of $(1.5 \text{ fm})^2 \text{ Hz}^{-1}$. In this experiment, we used a home-built interferometer operating at $\lambda = 1{,}064 \text{ nm}$ and with a light power of $\sim 1 \text{ mW}$ returned from a membrane with $m = 64 \text{ ng}$ and $\Gamma_m/2\pi = 20 \text{ Hz}$. The square root of the phase sensitivity, $\sqrt{S_{\varphi\varphi}^{im}}$, can be translated into a voltage sensitivity limit by division by the transfer function $|\chi^{tot}| \equiv \left|2k\chi_m^{eff}G\chi_{LC}\right|$ of the transducer. With the cooperativity chosen here, $\mathcal{C}_{em} = 150$, this corresponds to a voltage noise level of 60 pV $\text{Hz}^{-1/2}$ within the resonant bandwidth of this proof-of-principle transducer, but higher powers, and more sensitive optomechanical transduction[16,23] could readily improve this number. From our model, we furthermore deduce that the contribution of the thermal motion of the membrane adds an equal amount of voltage noise (Fig. 4b, green), such that, at this cooperativity, these noise contributions are balanced and their sum minimized to 84 pV $\text{Hz}^{-1/2}$.

Further analysis of the transducer noise has been performed by measurements with an additional, 'source', resistor, R_s, in series with the inductor of the circuit (Fig. 4c). The input to the circuit thus consists of the Johnson noise of both resistors, $(S_{VV}^{J})' = 2k_B(RT_R + R_sT_s)$. We cool the source resistor using liquid nitrogen, and optically measure the displacement of the membrane both at room ($T_s = 300 \text{ K}$) and at liquid nitrogen temperature ($T_s = 77 \text{ K}$). We can thus determine the amount of noise added by the transducer using the Y-factor method[24]. From equation (6), we expect to find a noise temperature of (Supplementary Information)

$$T_n = \left(\frac{1}{\eta_e} - 1\right)T_R + \frac{1}{\eta_e}\left(\frac{1}{\mathcal{C}_{em}}T_m + \frac{(1+\mathcal{C}_{em})^2}{\mathcal{C}_{em}}T_L\right) \quad (7)$$

at resonance, where the three summands are due to the Johnson noise of the circuit's loss, $R = 60 \Omega$, at $T_R = 300 \text{ K}$, the membrane's thermal fluctuations ($T_m = 300 \text{ K}$) and the noise in the optical readout ($T_L \approx 50 \text{ mK}$), respectively. We note that both the circuit's loading, $\eta_e = R_s/(R_s + R)$, and the cooperativity, $\mathcal{C}_{em} = R\mathcal{C}_{em}(R_s = 0 \text{ }\Omega)/(R_s + R)$, are now functions of the source resistance. In this experiment, we vary the cooperativity by varying the source resistor from $\mathcal{C}_{em}(R_s = 0 \text{ }\Omega) = 550$ to $\mathcal{C}_{em}(R_s = 2 \text{ k}\Omega) = 18$, and find a noise temperature consistent overall with equation (7), with the lowest measured value reaching down to 24 K (Fig. 4c).

The challenge of engineering a low-loss, overcoupled electronic resonance circuit ($\eta_e \to 1$) aside, the transducer itself adds only very little noise (green and yellow lines in Fig. 4c, representing the second and third terms in equation (7), respectively). For example, at a cooperativity of $\mathcal{C}_{em} = 70$ achieved with $R_s = 400 \text{ }\Omega$, subtracting the Johnson noise from the total noise yields optical quantum phase noise and membrane thermal noise temperatures of 4 K. Remarkably, the membrane contribution, which can usually only be suppressed by cryogenic cooling, is strongly reduced by the cooperativity parameter ($\propto T_m/\mathcal{C}_{em}$). The highest cooperativity we have obtained is $\mathcal{C}_{em} = 6{,}800$, by applying equation (3) to the data of Fig. 1c. This implies that membrane noise temperatures down to 40 mK can be expected, corresponding here to a voltage noise level of 5 pV $\text{Hz}^{-1/2}$.

For comparison, we performed measurements with an arrangement of ultralow-noise operational amplifiers connected directly to port 1. The amplifier is based on junction field-effect transistors (JFETs) and combines low input voltage noise (nominally 4 nV $\text{Hz}^{-1/2}$) with extremely low current noise (nominally 2.5 fA $\text{Hz}^{-1/2}$), as required[24] for measurements on a relatively high source impedance, which here amounts to $RQ_{LC}^2 \approx 140 \text{ k}\Omega$ at port 1. In practice, with a gain of 1,000, the best voltage sensitivity we have obtained is only $S_{VV}^{oa,tot}(\Omega_{LC}) = (130 \text{ pV})^2 \text{ Hz}^{-1}$ over the bandwidth of the LC resonance. Similar performance levels—on a par with the transducer discussed here—are expected even for ideal operation of other amplifiers described in the scientific and technical literature (Supplementary Information). Apart

from being competitive with standard electronics in its noise figures, our transducer provides a new functionality owing to its direct compatibility with fibre optical communication lines. The presented optoelectromechanical transducer also compares very favourably with previous proof-of-principle mechanical amplifiers for radio-frequency[25] and microwave[26] radiation (Supplementary Information).

Because our transducer noise floor is well below the room-temperature Johnson noise from the circuit's loss, $R = 60 \Omega$, this approach can be of particular relevance in applications where electronic Johnson noise is suppressed. For example, for direct electronic (quantum) signal transduction, the resonance circuit is overloaded ($\eta_e \to 1$) with a cold transmission line that carries the signal of interest, but no Johnson noise. In radio astronomy[27], highly efficient antennas looking at the cold sky can have noise temperatures far below room temperature. The usually required cryogenically cooled pre-amplifiers might be replaced by our transducer—a critical advantage for satellite missions—and extension to gigahertz frequencies should be straightforward using a.c. driving[4]. Direct and efficient conversion of radio-frequency signals into optics could save substantial resources in large phased-array antennas. Finally, in NMR experiments including imaging, cooled pickup circuits can deliver a significant sensitivity improvement, but this approach challenges present amplifier technology[28,29].

METHODS SUMMARY

The capacitor is fabricated by standard clean-room microfabrication techniques. Electrodes made of gold (200 nm thick) are deposited on a glass substrate and structured by ion-beam etching. Each segment is 400 μm long, with 60-μm gaps between the segments. Pillars ranging in height from 600 nm 1 μm are placed to define the membrane–electrode distance. The inductor is wound with Litz wires to ensure a high Q-factor. A variable trimming capacitor is used to tune the resonance frequency of the LC circuit.

The mechanical resonator consists of a 50-nm-thick aluminium layer on top of a high-stress stoichiometric SiN layer with a thickness of 100 or 180 nm depending on the sample. The aluminium layer is deposited on top of the whole wafer after the membranes have been released. Photolithography and chemical etching are subsequently used to remove the metal from the anchoring regions and from a circle in the middle of the membrane. The metal layer on SiN typically causes a 10% decrease in the eigenfrequency of the fundamental mode.

Optical interferometry is carried out using a commercial Doppler vibrometer (MSA-500 Polytec) and a home-made Michelson interferometer (for the data set in Fig. 4). The home-made Michelson interferometer uses shot-noise-limited, balanced-homodyne detection with a high-bandwidth (0–75 MHz) InGaAs receiver. The two d.c. outputs from the detector are used to generate the differential error signal, which is then fed to the piezoelectric actuator in the reference arm for locking the interferometer. The radio-frequency output of the detector is high-pass-filtered and fed to a spectrum analyser to record the vibrations of the membrane. Absolute calibration of the mechanical amplitude is carried out through a known modulation of the piezoelectric actuator at a frequency close to the mechanical peak.

1. Kippenberg, T. J. & Vahala, K. J. Cavity optomechanics: back-action at the mesoscale. *Science* **321**, 1172–1176 (2008).
2. Aspelmeyer, M., Kippenberg, T. J. & Marquardt, F. Cavity optomechanics. Preprint at http://arxiv.org/abs/1303.0733 (2013).
3. O'Connell, A. D. *et al.* Quantum ground state and single-phonon control of a mechanical resonator. *Nature* **464**, 697–703 (2010).
4. Teufel, J. D. *et al.* Circuit cavity electromechanics in the strong-coupling regime. *Nature* **471**, 204–208 (2011).
5. Faust, T., Krenn, P., Manus, S., Kotthaus, J. & Weig, E. Microwave cavity-enhanced transduction for plug and play nanomechanics at room temperature. *Nature Commun.* **3**, 728 (2012).
6. Gröblacher, S., Hammerer, K., Vanner, M. R. & Aspelmeyer, M. Observation of strong coupling between a micromechanical resonator and an optical cavity field. *Nature* **460**, 724–727 (2009).
7. Verhagen, E., Deléglise, S., Weis, S., Schliesser, A. & Kippenberg, T. J. Quantum-coherent coupling of a mechanical oscillator to an optical cavity mode. *Nature* **482**, 63–67 (2012).
8. Taylor, J. M., Sørensen, A. S., Marcus, C. M. & Polzik, E. S. Laser cooling and optical detection of excitations in a LC electrical circuit. *Phys. Rev. Lett.* **107**, 273601 (2011).
9. Regal, C. A. & Lehnert, K. W. From cavity electromechanics to cavity optomechanics. *J. Phys. Conf. Ser.* **264**, 012025 (2011).

10. Safavi-Naeini, A. H. & Painter, O. Proposal for an optomechanical traveling wave phonon-photon translator. *New J. Phys.* **13,** 013017 (2011).
11. Wang, Y.-D. & Clerk, A. A. Using interference for high fidelity quantum state transfer in optomechanics. *Phys. Rev. Lett.* **108,** 153603 (2012).
12. Stannigel, K., Rabl, P., Sorensen, A. S., Zoller, P. & Lukin, M. D. Optomechanical transducers for long-distance quantum communication. *Phys. Rev. Lett.* **105,** 220501 (2010).
13. Dong, C., Fiore, V., Kuzyk, M. C. & Wang, H. Optomechanical dark mode. *Science* **338,** 1609–1613 (2012).
14. Palomaki, T. A., Harlow, J. W., Teufel, J. D., Simmonds, R. W. & Lehnert, K. W. Coherent state transfer between itinerant microwave fields and a mechanical oscillator. *Nature* **495,** 210–214 (2013).
15. Bochmann, J., Vainsencher, A., Awschalom, D. D. & Cleland, A. N. Nanomechanical coupling between microwave and optical photons. *Nature Phys.* **9,** 712–716 (2013).
16. Thompson, J. D. *et al.* Strong dispersive coupling of a high finesse cavity to a micromechanical membrane. *Nature* **452,** 72–75 (2008).
17. Andrews, R. W. *et al.* Reversible and efficient conversion between microwave and optical light. Preprint at http://arxiv.org/abs/1310.5276 (2013).
18. Truitt, P. A., Hertzberg, J. B., Huang, C. C., Ekinci, K. L. & Schwab, K. C. Efficient and sensitive capacitive readout of nanomechanical resonator arrays. *Nano Lett.* **7,** 120–126 (2007).
19. Unterreithmeier, Q. P., Weig, E. M. & Kotthaus, J. P. Universal transduction scheme for nanomechanical systems based on dielectric forces. *Nature* **458,** 1001–1004 (2009).
20. Weis, S. *et al.* Optomechanically induced transparency. *Science* **330,** 1520–1523 (2010).
21. Ilchenko, V. S. *et al.* K_a-band all-resonant photonic microwave receiver. *IEEE Photonics Technol. Lett.* **20,** 1600–1612 (2008).
22. Devgan, P. S., Pruessner, M. W., Urick, V. J. & Williams, K. J. Detecting low-power and RF signals and using a multimode optoelectronic and oscillator and integrated optical filter. *IEEE Photonics Technol. Lett.* **22,** 152–154 (2010).
23. Anetsberger, G. *et al.* Near-field cavity optomechanics with nanomechanical oscillators. *Nature Phys.* **5,** 909–914 (2009).
24. Horowitz, P. & Hill, W. *The Art of Electronics* 2nd edn, 428–454 (Cambridge Univ. Press, 1989).
25. Jensen, K., Weldon, J., Garcia, H. & Zettl, A. Nanotube radio. *Nano Lett.* **7,** 3508–3511 (2007).
26. Massel, F. *et al.* Microwave amplification with nanomechanical resonators. *Nature* **480,** 351–354 (2011).
27. Kraus, J. D. *Radio Astronomy* (McGraw, 1966).
28. Kovacs, H., Moskau, D. & Spraul, M. Cryogenically cooled probes—a leap in NMR technology. *Prog. Nucl. Magn. Reson. Spectrosc.* **46,** 131–155 (2005).
29. Resmer, F., Seton, H. C. & Hutchison, J. M. Cryogenic receive coil and low noise preamplifier for MRI at 0.01 T. *J. Magn. Reson.* **203,** 57–65 (2010).
30. Yu, P.-L., Purdy, T. P. & Regal, C. A. Control of material damping in high-Q membrane microresonators. *Phys. Rev. Lett.* **108,** 083603 (2012).